Selective Hydrolysis by Engineered Cutinases

Characterization of Aliphatic-Aromatic Homo and Co-Polyesters by LC and LC–MS Methods

Abdelraheem, E.; Tseliou, V.; Desport, J.; Serizawa, M.; Schürmann, M.; Buijsen, P.; Peters, R.; Gargano, A.F.G.; Mutti, F.G.

DOI
10.1002/chem.202403879

Publication date
2025

Document Version
Final published version

Published in
Chemistry - A European Journal

Chemistry–A European Journal
Research Article
doi.org/10.1002/chem.202403879
Chemistry Europe
European Chemical Societies Publishing
www.chemeurj.org

Selective Hydrolysis by Engineered Cutinases: Characterization of Aliphatic-Aromatic Homo and Co-Polyesters by LC and LC–MS Methods

Eman Abdelraheem[+,[a]] Vasilis Tseliou[+,[a]] Jessica Desport,[[a]] Masashi Serizawa,[[a]] Martin Schürmann,[[b]] Paul Buijsen,[[c]] Ron Peters,[[a, c]] Andrea F. G. Gargano,*[[a]] and Francesco G. Mutti*[[a]]

The performance, biodegradability, and recyclability of polymers can be tuned during synthesis by adopting monomers with different chemical characteristics. Recent research has shown the aptness of some hydrolases to depolymerize polyesters under mild conditions compared to chemical approaches. Herein, we engineered a cutinase from *Thermobifida cellulosilytica* (Tc_Cut2NV^{WCCG}) for improved thermostability (up to 91 °C) and compared it with previously reported leaf-branch compost cutinase (LCC^{WCCG}) for the hydrolysis of low molar mass substrates, as well as aliphatic and aromatic homo- and co-polyesters. For both enzymes, higher hydrolysis rates were observed for aliphatic compared to aromatic homo-polyesters. SEC-MS analysis revealed that the hydrolysis of aliphatic/aromatic co-polyesters occurred at the aliphatic monomers, significantly reducing the molecular weight and changing the end-group composition. These results underline the importance of co-polymer composition in the biodegradation of co-polymer systems and demonstrate the applicability of enzymes for the analytical characterization of synthetic polymers by selectively reducing their molecular weight. Finally, the discovery and engineering of highly active enzymes that can efficiently hydrolyze a wide variety of synthetic polyesters create new opportunities for their efficient recycling under mild conditions.

Introduction

The chemical composition of polymers (i.e., types of end groups, co-polymer ratio, molecular weight) is an important parameter for determining their mechanical properties, including degradability and melting point.[1] A detailed understanding of polymer composition is pivotal to designing materials that offer improved recyclability and controlled biodegradation.[2] Therefore, the development of catalytic methods that enable controlled polymer depolymerization is of high interest for applications in polymer recycling and analytical chemistry that aim to characterize polymer distribution. The physical and chemical degradation of polymers includes thermal, photo-chemical, mechanochemical, and oxidating processes.[3] These processes can successfully degrade the polymer but lack selectivity.

In contrast, enzymes offer the potential for chemoselective degradation of polymers by targeting specific bonds. Moreover, enzymes can display different hydrolytic kinetics for different monomers depending on the neighboring monomer within the polymer sequence. Therefore, available and novel hydrolases could be applied to characterize the microstructure of synthetic polymers similarly to what is done for the characterization of proteins (i.e., chemoselective digestion).

The capability of some hydrolases to degrade synthetic polyesters has been investigated over the past two decades, leading to the discovery and engineering of variants that can fully degrade polyethylene terephthalate (PET) and, therefore, potentially be used for recycling and bioremediation purposes. The enzymes used for this purposes were cutinases isolated from microbial strains (e.g. *Ideonella sakaiensis* and *Thermobifida fusca*) or fungi (*Fusarium solani*, *Humicola insolens*, and *Aspergillus oryzae*), and further engineered ones.[4] Among the recently published candidates enzymes for PET hydrolysis are *Thermobifida fusca* cutinase (TfCut2),[5] *Thermobifida cellulosilytica* cutinase 1 (ThcCut1)[6] and an engineered leaf-branch compost cutinase (LCC^{WCCG}).[7] Further recent research has also led to the discovery and engineering of other catalytically active and thermostable enzymes for the depolymerization of PET.[8]

However, these recent works on polyester degradation by enzymes has mainly focused on methods to degrade homopolymers back to the starting monomers. Müller et al. have studied the process of co-polyesters hydrolysis, revealing that the

[a] E. Abdelraheem,[+] V. Tseliou,[+] J. Desport, M. Serizawa, R. Peters, A. F. G. Gargano, F. G. Mutti
van 't Hoff Institute for Molecular Science, University of Amsterdam, Science Park 904, 1098 XH Amsterdam, the Netherlands
E-mail: a.gargano@uva.nl
f.mutti@uva.nl
[b] M. Schürmann
InnoSyn B.V., Urmonderbaan 22, 6167 RD Geleen, the Netherlands
[c] P. Buijsen, R. Peters
Covestro Resins & Functional Materials, Sluisweg 12, 5145 PE Waalwijk, the Netherlands
[+] These authors contributed equally to this work.

Supporting information for this article is available on the WWW under https://doi.org/10.1002/chem.202403879

cleavage rates are dependent on the heterogeneity of the polymer as well as the chemical structure and molecular environment (crystallinity) in which the ester bonds are embedded.[9] Yet, to date, analytical investigations studying the changes of chemical structures in co-polymers as a result of enzymatic degradation are lacking. Herein, we report the development and use of cutinases to depolymerize model homo- and co-polyesters. Two enzymes were investigated for their selectivity in the hydrolysis of small molecules and structurally diverse polyesters. One of these enzymes was engineered from the cutinase family to improve its thermostability and allow depolymerization reactions at higher temperatures in aqueous buffer media. The other studied cutinase was a previously reported variant from the leaf-branch compost cutinase (LCC).[7]

Various LC and LC–MS methods were applied to characterize the products and the remaining polymer after the enzymatic hydrolysis. An overview of the steps performed is presented in SI, Figure S1. We selected polyesters with different physical and chemical properties composed by different monomers (Figure 1): polyester 1 (PES1) (green box) as an aliphatic polymer based on dodecanedioic acid (DDA, 50%, **2**) and ethylene glycol (EG, 50%, **1**); PES2 (orange box) as a co-polymer with four different monomer units randomly distributed, namely, terephthalic acid (TPA, 37%, **3**), isophthalic acid (IPA, 12%, **4**), neopentyl glycol (NG, 48%, **6**) and adipic acid (ADA, 3%, **5**); PES3 (blue box, commonly indicated as PET) as an aromatic polymer based on terephthalic acid (TPA, 50%, **3**) and ethylene glycol (EG, 50%, **1**); and PES 4 (violet box) as an aromatic polymer based on terephthalic acid (TPA, 50%, **3**) and neopentyl glycol (NG, 50%, **6**). These polyesters were also selected for their industrial relevance as part of the next generation of polymers. The synthesis of these polyesters was undertaken as part of this study, with detailed procedures for their synthesis and characterization provided in the Supporting Information (SI).

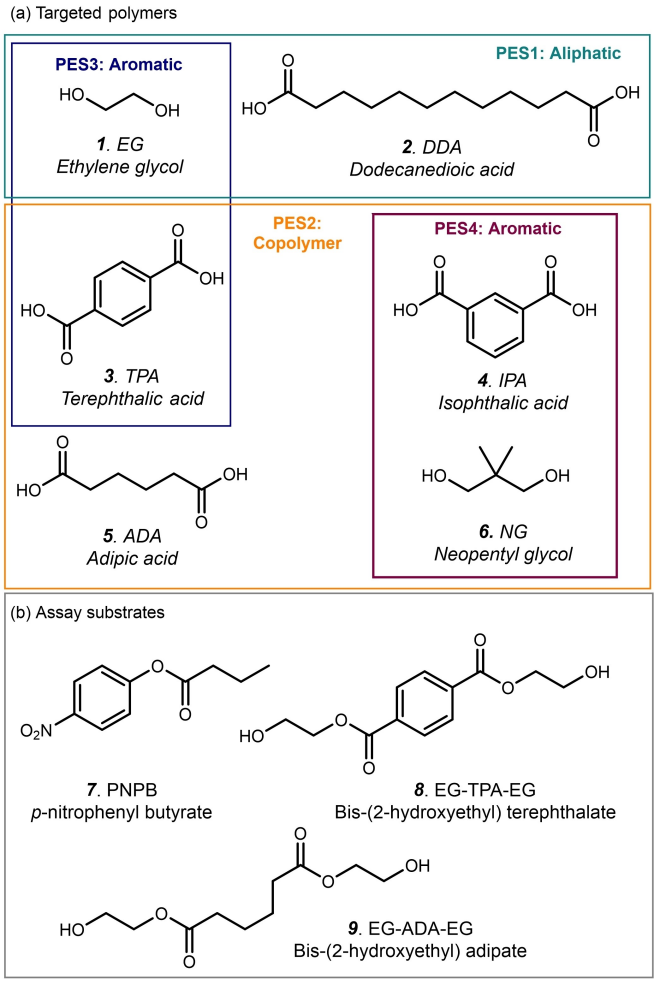

Figure 1. a) Structures of the monomers composing the polymers enzymatically hydrolyzed and b) assay substrates used in this study. The MW of the polymers was determined using SEC against polystyrene standards.

Results and Discussion

Selection and Engineering of Thermostable and Chemoselective Enzymes for the Hydrolysis of Polyesters

We selected a variant of a leaf-branch compost cutinase (LCC^{WCCG}) for its ability to depolymerize PET polyesters (PES),[7,8] and a variant of a cutinase from *Thermobifida cellulosilytica* (Tc_Cut2 R29 N A30 V; herein referred as Tc_Cut2NV) for its catalytic activity toward PET and polylactic acid (PLA).[10] *p*-Nitrophenyl butyrate (PNPB, **7**) was used as assay substrate to determine the specific activity of both enzymes at 40 °C. Although this work aimed at targeting the hydrolysis of insoluble polymers, **7** is the commonly used substrate for initial evaluation of the catalytic performance of this type of hydrolytic enzymes. LCC^{WCCG} and Tc_Cut2NV showed 11828 U mg^{-1} and 9904 U mg^{-1} specific activity, respectively.

As the depolymerization reaction rates for the polyesters increased at higher temperatures, we hypothesized that the reactions could be run at a temperature closer to the glass transition temperature (Tg) of the polymers, therefore increasing polymer chain accessibility (Tg, between 58 and 87 °C, SI Table S2, Figure S6).[11] We therefore attempted to increase the thermostability of Tc_Cut2NV (>60 °C). Tc_Cut2NV (PDB: 5LUK) has a high structural similarity with the high thermostable variant LCC^{WCCG} (PDB: 4EB0 for wild-type LCC). Both Tc_Cut2NV and wild-type LCC display a typical α/β-hydrolase fold in which nine antiparallel β-strands are enveloped by ten α-helices, five from each side.[7,12] The enzymes contain an active site serine residue (S131 for Tc_Cut2NV and S138 for LCC) along with the proximal aspartic acid and histidine residues that create a catalytic triad, which is essential for hydrolysis. Figure 2a depicts the X-ray crystal structure of Tc_Cut2NV where the catalytic triad is highlighted (magenta), whereas Figure 2b displays a structural alignment between Tc_Cut2NV (grey) and wild-type LCC (magenta). Due to their high structural similarity, we speculated that introducing similar mutations of the variant LCC^{WCCG} to the scaffold of Tc_Cut2NV might also increase the thermal stability of the latter. Therefore, via 3D-structural alignment, the corresponding residues were identified in the

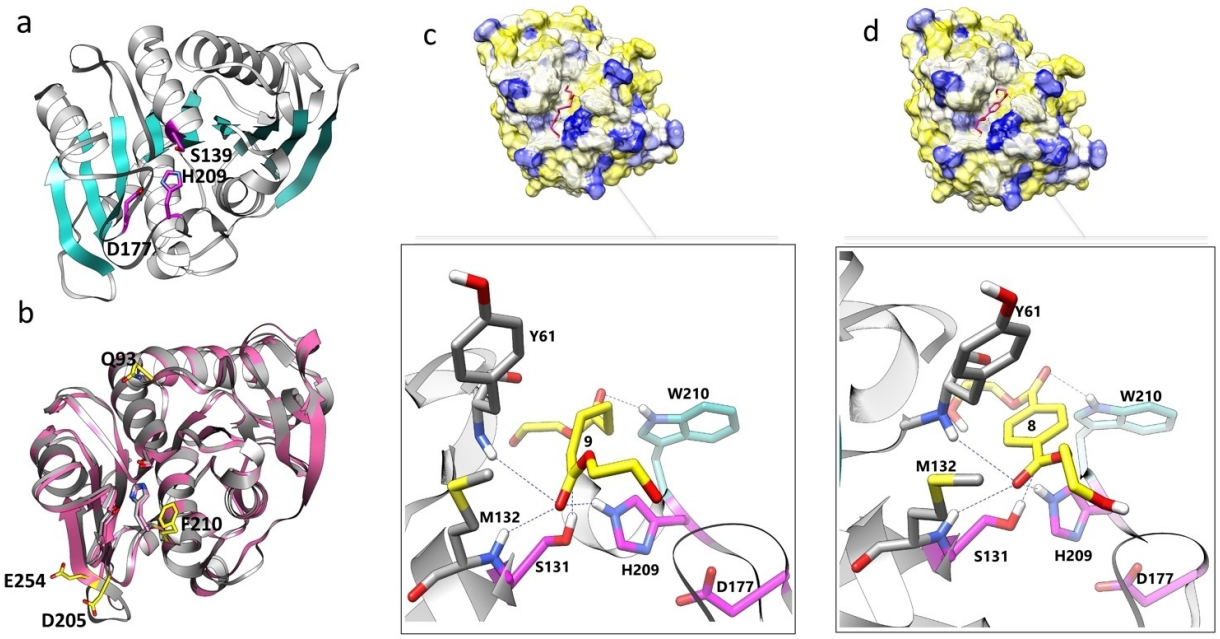

Figure 2. a) X-ray crystal structure of the Tc_Cut2NV (PDB: 5LUK) in which nine antiparallel β-strands (green) are enveloped by ten α-helices displaying a typical α/β-hydrolase fold. The catalytic triad is shown in magenta. B) X-ray crystal structure of wild-type LCC (PDB: 4EB0, magenta) superposed with Tc_Cut2NV. The corresponding residues in Tc_Cut2NV scaffold that generated increased thermostability in the LCC^{WCCG} variant are shown in yellow. c-d) Docking studies with enzyme Tc_Cut2NV^{WCCG} as receptor and using (c) aliphatic model substrate **9** or (d) aromatic model substrate **8**. The enzyme surface is depicted in blue and yellow to refer to hydrophilic and hydrophobic amino acid residues, respectively. The structures highlight the distance (<3 Å) between the catalytic S131 residue and the reactive carbon atom of the model substrates. H209 and the mutated residue W210 are involved in hydrogen bonds with the oxygen atoms of the respective carbonyl moieties at distances of 3–4 Å. Y61 and M132 are the amino acid residues that make up the oxyanion hole. The N–H moieties of the backbone amide groups of Y61 and M132 interact with the oxygen atom of the reacting carbonyl group of the substrate. All these interactions occur at distances of 3–4 Å. The catalytic triad is shown in magenta, and mutations in light green. Docking was performed using YASARA structure, and Chimera software was used for structural alignment and visualization.

Tc_Cut2NV scaffold and the mutations (Q93G, D205C, F210W and E254C) were introduced to create the Tc_Cut2NV^{WCCG} gene, which was recombinantly expressed in *E. coli* and the enzyme was purified by Ni^{2+}affinity chromatography (SI, Figure S2) as previously done for Tc_Cut2NV and LCC^{WCCG}. In a first round of purification, Tc_Cut2NV^{WCCG} was obtained with approximately 95% purity, with the only impurity being a high molecular weight co-eluting protein from the *E. coli* BL21(DE3) host organism. A second round of purification demonstrated that enzyme purity could be increased to >99% by completely eliminating the co-eluting protein (SI, Figure S2B). Tests of depolymerization on PES1 and PES4 unequivocally showed no difference when using Tc_Cut2NV^{WCCG} at ca. 95% purity compared to >99% purity (SI, Figure S19). Therefore, the preparation at ca. 95% enzyme purity was used throughout this study.

Thermostability measurements revealed that the mutations in the Tc_Cut2NV^{WCCG} scaffold enhanced the stability of the enzyme, which displayed an impressive melting temperature (Tm) of 91 °C (~27 °C higher than the parental Tc_Cut2NV) (SI, Figure S3). The new variant also showed a 16% increase in catalytic activity for the hydrolysis of the assay substrate **7** compared with the Tc_Cut2NV (11460 U mg^{-1} and 9904 U mg^{-1} for Tc_Cut2NV^{WCCG} and Tc_Cut2NV, respectively). These results motivated us to conduct long-term thermostability measurements at 40 °C and, for up to 6 days, at 71 °C using purified Tc_Cut2NV^{WCCG}. The enzyme showed a similar specific activity for substrate **7** at 71 °C and at 40 °C (ca. 5000 U mg^{-1}) at the beginning, but its activity at 71 °C decreased 1.6-fold and 6-fold after 3 and 6 days, respectively (Table 1).

Next, we tested whether the introduced mutations improved the tolerance of the enzyme against organic solvents. We chose hexafluoro-2-propanol (HFIP) and tetrahydrofuran (THF) because these solvents can solubilize polyesters, thereby making it possible to increase the accessibility of their chains. Unfortunately, the catalytic activity of Tc_Cut2NV^{WCCG} decreased 30-fold or 40-fold at the tested concentration of added HFIP (10–90% v v^{-1}) (SI, Table S1) or THF (50%). This outcome indicated that none of these solvents could be used in the enzymatic depolymerization reactions. Therefore, we decided to conduct all reactions in aqueous buffers without any organic cosolvent.

Activity Test with Assay Substrates and Structural Insights on Catalytic Activity and Selectivity

Next, we assessed whether the enzymes could accept both aliphatic and aromatic low molar mass substrates by combining wet-lab experiments and computational docking simulations. We used bis-(2-hydroxyethyl) terephthalate (**8**) (EG-TPA-EG) and bis-(2-hydroxyethyl) adipate (**9**) (EG-ADA-EG) (NMR data in SI,

Table 1. Long-term thermostability measurements with Tc_Cut2NV^{WCCG} or LCC^{WCCG} with assay substrate **7** at 71 °C.

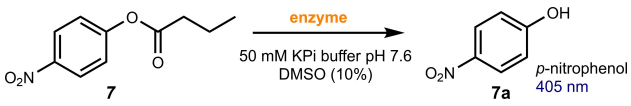

Entry	Enzyme	Time (days)	Activity[a] (U mg^{-1})
1	Tc_Cut2NV^{WCCG}	0	4913
2	Tc_Cut2NV^{WCCG}	3	3003
3	Tc_Cut2NV^{WCCG}	6	807
4	LCC^{WCCG}	0	6735
5	LCC^{WCCG}	3	5345
6	LCC^{WCCG}	6	660

[a] Activity was measured by monitoring the increase of the absorbance of **7a** at λ of 405 nm for 1 min using the extinction coefficient (ε_{405nm} = 9.36 mL/(μmol*cm)). Reactions were performed with **7** (4 mM) at 71 °C in 50 mM KPi pH 7.6 with the purified enzymes. Measurements were carried out using a spectrophotometer equipped with temperature control. In all measurements, the enzymes were incubated at the desired temperature prior to the assay.

Figure S5) as assay substrates because these are structurally similar to the targeted polyesters and therefore offer a simplified testbed for our studies.[13] Although these experiments do not account for the restricted molecular accessibility typical of solid materials, they accurately reflect the enzyme's propensity for hydrolysis. Molecular docking simulations using either **8** or **9** as substrates revealed that both Tc_Cut2NV^{WCCG} and LCC^{WCCG} are receptors. Moreover, in the computational models showing the substrate in a productive binding pose, the catalytically active serine (S131 for Tc_Cut2NV^{WCCG} or S165 for LCC^{WCCG}) was found to be in close proximity to the reactive carbon of the substrate's carbonyl group (< 3 Å) (Figure 2c and SI, Figure S4).

The molecular docking poses in the productive binding modes show the influence of the catalytic histidine residue (H209 for Tc_Cut2NV^{WCCG} and H242 for LCC^{WCCG}) on the protonation of the oxygen atom of the carbonyl group involved in the hydrolysis reaction, which is situated approximately 4 Å away. Additionally, stabilizing interactions occur between the same oxygen atom and the N–H moieties of the backbone amide groups of Y61 and M132 (Tc_Cut2NV^{WCCG} residue numbering), which make up the oxyanion hole; these interactions are observed at distances of 3–4 Å. Notably, the introduced tryptophan mutation (F210W for Tc_Cut2NV^{WCCG} or F243W for LCC^{WCCG}) must influence the positioning of the low molar mass substrates in the active site through the possible formation of a hydrogen bond between the NH moiety of the tryptophan residue and the oxygen atom of the second carbonyl (i.e., not involved in the hydrolysis) of the substrate (See Figure 2).

As predicted by the docking studies, both Tc_Cut2NV^{WCCG} or LCC^{WCCG} could hydrolyze the test low molar mass substrates. After 1 or 24 h, we detected the formation of monomer **3** or **5** by LC–MS as the products of the depolymerization of assay substrates **8** or **9**, respectively. Within the investigated timeframe (up to 24 h) for the depolymerization of **8** or **9**, LCC^{WCCG} produced a greater amount of the monomer **3** or **5** (near 100% hydrolysis) compared with Tc_Cut2NV^{WCCG} (SI, Figure S11; around 80% of hydrolysis). Notably, using Tc_Cut2NV^{WCCG}, we detected the formation of partially hydrolyzed intermediates, thus maintaining one of the two ester moieties (compound **8a** and **9a** of SI Figure S11). In contrast, both intermediates were consumed by LCC^{WCCG} after 30 min of reaction. These observations indicate a different reactivity between Tc_Cut2NV^{WCCG} and LCC^{WCCG}, with the latter enzyme being more catalytically active. Moreover, the hydrolysis of the aliphatic low-molar-mass substrate **9** catalyzed by LCC^{WCCG} was significantly faster than that of the aromatic low-molar-mass substrate **8** within the first 100 min of the reaction.

Analysis of the Depolymerization of Homopolymers PES1, PES3 and PES4 by RPLC-UV-MS and SEC-UV

After elucidating the different reactivity of Tc_Cut2NV^{WCCG} and LCC^{WCCG} for the hydrolysis of small molecules and assay substrates, we applied the enzymes to the depolymerization of polyesters. The enzymes developed were used to analyze an aliphatic, PES1 (DDA-EG, **2**–**1**, Mw = 17 kDa), as well as the aromatic PES3 (TPA-EG, **3**–**1**, Mw = 132 kDa) and PES4 (IPA-NG, **4**–**6**, Mw = 14 kDa), homo-polyester synthetic models (Figure 1). PES3 and PES4, which exhibit significant differences in molecular weight, were used to assess the influence of this parameter on depolymerization. The polymer samples used in this study were solid materials in different forms such as powder/ granules (PES 1,2,4), or blocks (PES3). The polymers were hydrolyzed as solid dispersions in water. However, for most of the polymers, the reaction temperature of 71 °C exceeded their glass transition temperature (T_g), except for PES3 (see Table S2). Above the T_g, the amorphous regions of polymers exhibit increased molecular mobility and are more susceptible to enzymatic attacks due to the greater free volume available for diffusion, thereby facilitating depolymerization.[14] Moreover, different strategies to increase the surface area were applied and are described in the SI Figures S7 and S13.

Two methods were used to characterize the hydrolysis products: RPLC-UV-MS to monitor the release of dicarboxylic acid monomers in the aqueous reaction mixture (**3** for PES3 and **2** for PES1) and SEC-UV to analyze the remaining polymer material after centrifugation, sample evaporation, and redissolution in HFIP. Details of the RPLC and SEC analysis are presented in Figures S14, S15 and S17.

Figure 3a illustrates the molecular weight distribution (relative to polystyrene standards) as Log MW plots obtained for the depolymerization reactions of PES1 by LCC^{WCCG} and Tc_Cut2NV^{WCCG} after different reaction times. Negative control experiments (i.e., devoid of enzyme, grey trace) were also performed. We observed complete depolymerization of PES1 with LCC^{WCCG} after 30 min (yellow trace) as the polymer distribution area disappeared. In the case of Tc_Cut2NV^{WCCG} (blue trace), the PES1 polymer peak decreased in 30 min and

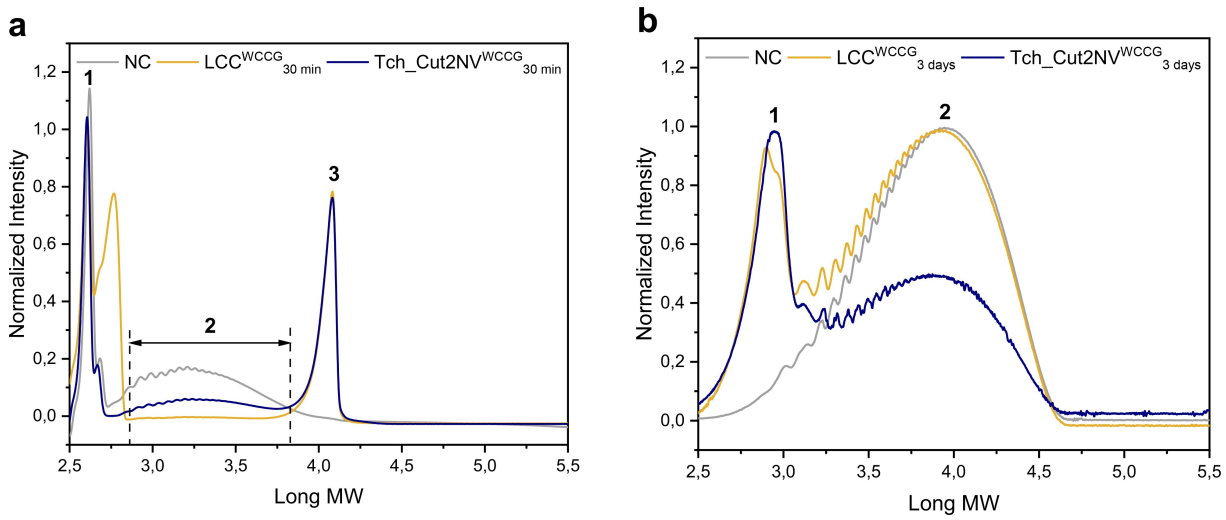

Figure 3. Enzymatic hydrolysis of model polymers PES1 and PES4 catalyzed by Tc_Cut2NV^{WCCG} or LCC^{WCCG}. Reactions were performed with 1 mg PES1 and 1 mg PES4, 1 μM of enzymes at 71 °C in 50 mM KPi. (a) Size exclusion chromatography (SEC) profile of the PES1 samples (polystyrene equivalents) after 30 min incubation using LCC^{WCCG} (yellow trace) and Tc_Cut2NV^{WCCG} (blue trace); PES1 displayed degradation compared with the negative control without enzymes (grey trace) and complete depolymerization was detected within less than 24 h; 1 indicates the elution area of salts and low molecular weight components, 2 indicates the polymer elution area, and 3 indicates the peak of the enzyme used for the depolymerization; the increase of low molecular weight species 1 with almost no change in molecular weight distribution was observed as a result of polymer degradation. LCC^{WCCG} appear to degrade the polymer much faster than Tc_Cut2NV^{WCCG} with no residual polymer present after 30 min of incubation. (b) SEC profile of PES4 solution in THF using LCC^{WCCG} (yellow trace) and Tc_Cut2NV^{WCCG} after 1 day of incubation; 1 indicates the elution area of salts and low molecular weight components, whereas 2 indicates the polymer elution area. For both a) and b) the intensities are normalized to the highest peak to facilitate the comparison. Data obtained from the analysis of released monomers from PES1–3 are reported in Figure S17.

the complete depolymerization was observed within less than 24 h. The process went hand in hand with the progressive formation of **2** as observed by RPLC-MS and the visual observation of the complete degradation of PES1 in the reaction mixture.

In the case of the aromatic polymers PES3 and PES4, limited amount of **3** or **4**, respectively, was released in the first 24 h of reaction time. Consequently, the reaction time was extended to 3 days, yet even after this period, the reaction remained incomplete. (results are presented in Figure SI–17). This result suggests that the enzymes exhibit greater catalytic activity for aliphatic polyesters, as the aliphatic polyester was hydrolyzed in a much shorter time frame (in less than 1 h for both enzymes). SEC-UV analysis showed a different variation in the polymer area for PES4 compared to PES3 after 3 days of enzymatic degradation (PES3: 24% vs. 16% with LCC^{WCCG} and Tc_Cut2NV^{WCCG}, respectively; PES4: 20% vs. 33% with LCC^{WCCG} and Tc_Cut2NV^{WCCG}, respectively). This may suggest differences in hydrolysis rates related to the polymer's molecular weight; however, other factors, such as the distribution of the polymer within the solid matrix, may also play a role. Further investigation using time-course sampling and a quantitative analysis of polymer distribution is needed to draw definitive conclusions.

Despite the significant release of monomer recorded by RPLC-UV-MS and the formation of small MW species observed in SEC-UV over the reaction time, we noticed negligible changes in the molecular weight distribution for both PES3 and PES4. Therefore, we conclude that for all homopolymers, the hydrolysis occurred primarily at the end groups of the polymers with no/ limited chain hydrolysis of the polymer chains.

Molecular Characterization of PES2 LCC Hydrolysis by SEC-MS

Finally, we applied the enzymatic depolymerization reactions discussed above to the aromatic-aliphatic co-polyester PES2, which is a randomly distributed co-polymer made of 49% aromatic acid monomer (TPA + IPA, **3** + **4**), 3% aliphatic acid monomer (ADA, **5**) and one alcohol (NG, **6**) (further details in Figure 1 and Table S2).

Our analysis focused on the depolymerization of co-polymer PES2 for 6 days with 1 μM LCC^{WCCG} or Tc_Cut2NV^{WCCG} compared to the negative control.[15] RPLC-UV and SEC-UV results from the hydrolysis of the polymer using LCC^{WCCG} and Tc_Cut2NV^{WCCG} can be found in SI Figure S16 and S18. RPLC-UV results revealed a slow hydrolytic behavior of PES2, similar to that of PES3. However, unlike for the homopolymer PES3 and PES4, SEC-UV analysis of the unsoluble polymer revealed that PES2_LCC sample (i.e., depolymerization of PES2 by LCC^{WCCG}) presented a significant reduction in molecular weight (Mn from 9748 to 6223 and Mw from 16809 to 11824). Limited MW reduction was observed for the PES2 sample treated with Tc_Cut2NV^{WCCG} (Mn from 9748 to 9480 and Mw from 16809 to 16170).

To identify the monomer composition of the species detected by SEC-UV and elucidate possible chemical composition changes, the degradation products – insoluble in the reaction media – were solubilized in THF and analyzed by SEC-UV/ESI-MS.[16] While UV detection provided information on the

entire polymer molecular weight distribution, as shown in Figure 4a, MS hyphenation enabled the identification of the chemical composition of a wide range of oligomers (up to 5300 Da). Due to health hazards and ESI compatibility, we adopted THF as the solvent for the SEC-MS analysis. Similar profiles were observed between SEC in THF and HFIP for this polymer. It has to be noted that MS analysis cannot be considered quantitative as the analysis reflects chemical composition only of the low MW components of the polymers, and as different chemical composition may have different MS ionization efficiency (e.g. cyclic species are known to be overestimated with respect to other end group). However, this technique is applied to qualitative capture changes in chemical composition.[17]

A systematic data analysis approach was applied to the MS spectra recorded during SEC separation. For clarity, only a fraction of the mass spectra is depicted in Figure 4a (signals sum from 8 to 9 min of SEC elution) and only the results for the samples treated with LCC^{WCCG} and the negative control are reported. Details of the assignments as well as data for PES2 treated with Tc_Cut2NV^{WCCG} are provided in the SI (Figure S20 and S21; Table S4 to S5). Results with Tc_Cut2NV are not discussed as we observed a lower level of hydrolysis with this enzyme.

Our data analysis revealed two important changes in PES2 upon hydrolysis by LCC^{WCCG}: (i) changes in polymer end groups and (ii) changes in monomer composition.

Polyesters exhibit different end-group compositions depending on how they have been synthesized.[16,18] The mass spectra obtained from the original polymer sample PES2_NC (control experiment for PES2 with no enzyme in the media (Figure 4b,c) features three different end-group types – i.e., di-acid, mono-acid, di-alcohol – as well as cyclic chains (lacking end-group contribution in their mass). The cyclic, di- and mono-acid terminated chains are the most abundant signals in the spectra of the starting material making 85% of the sum of the monoisotopic peaks (51% being cyclics, 34% mono-acid, 14% di-acid and 1% di-alcohol terminated). These results only partially agree with NMR data where acid end-groups accounted for ca. 14 mol% over the MW range (Table S2). Because of known ionization yields differences of end groups in ESI-MS, it is not possible to comment on the relative abundance of oligomers as a function of their chain-end in the same sample. However, it is possible to assess differences in their relative contributions between samples. In particular, the MS signature

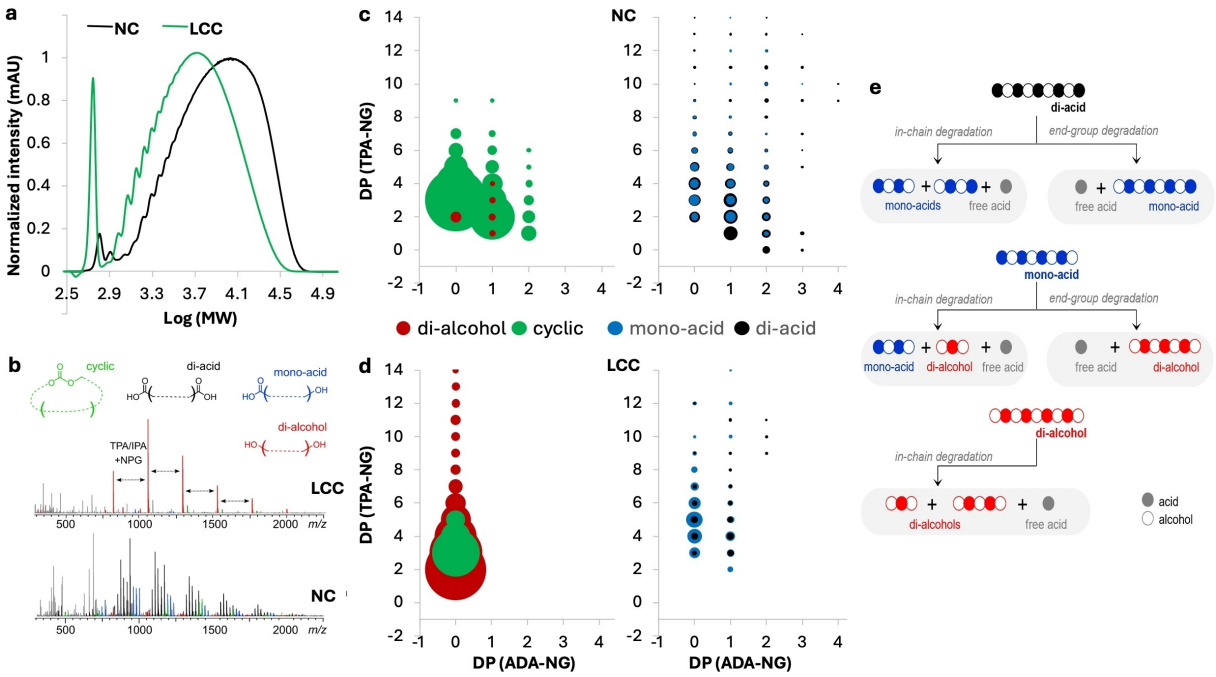

Figure 4. a): Molecular weight distributions of PES2_control (NC, black trace) and after hydrolysis using LCC^{WCCG} (LCC, green). The log MW is acquired via SEC-UV and relative to polystyrene standards (SI, Figure S9). b) From top to bottom, respectively, mass spectra averaged over 1 min of SEC elution (8 to 9 min) for PES2 depolymerized with LCC^{WCCG} (LCC) and its control experiment (NC). MS peaks are assigned to a given end-group pair by color: mono-acid (blue), di-acid (black), di-alcohol (red) and cyclic (green). The grey signals are assigned to background noise and sodium iodide (NaI) clusters. All peaks above 0.2% intensity were processed in a semi-automated fashion using MSPolyCalc[19] and based on the known polymer compositions. The data processing resulted in molecular formula assignments within a mass tolerance of 5 ppm and with good isotopic pattern match (within 95% similarity for isotopic zones up to A+3). All species were detected in positive ion mode as $[M+zNa]^{z+}$ sodium adducts with charge states (z) ranging from 1 to 3. c,d) Bubble chart reporting the assigned molecular formula from the SEC-MS analysis as a function of the number of polymer units (degree of polymerization, DP) of aromatic-based monomers (TPA/IPA-NPG; **3,4–5**) versus aliphatic monomers (ADA-NPG; **2–5**) for (c) PES2_LCC and (d) PES2_control. The dimension of the bubbles is scaled with the maximum intensity in the MS plot (alternative representation in SI, Figure S20 and 21, data available in SI Table S4–5). e) Schematic representation of polymer chain degradation as a function of types of end groups. We define 'end group degradation' as cleavage events occurring at the terminus of a polymer chain, resulting in the formation of a shorter chain with a di-alcohol end group. 'In-chain degradation' refers to cleavage events that occur within the internal regions of the polymer chain, potentially leading to the formation of two shorter chains, one with an acid end group and the other with di-alcohol end groups.

of the degraded PES2_LCC sample (Fig. 4 d) differs significantly from the MS profile of the original polymer. Here signals assigned to di-alcohol-terminated chains are predominant, with 88% of the sum of the monoisotopic peak intensities. The secondary most abundant signals were assigned to cyclic oligomers, while peaks assigned to mono- and di-acid terminated chains were in the minority, with intensities of 10% and 2% maximum, respectively. Experiments by changing the ionization additive from sodium to ammonium revealed similar end-group changes.

Additionally, after hydrolysis, almost all the cyclic polymers disappeared, suggesting that they were hydrolyzed into linear polymers. Figure 4e illustrates the proposed mechanism of degradation that results in the release of di-acids from variable polyester chains as a function of their end-group type. As illustrated, the hydrolysis process gradually leads to the release of acid terminated monomers and the fully alcohol-terminated polymer chains, regardless of the localization of the cleavages (i.e., at the end of, or within the chain).

The composition of the oligomers in terms of aromatic and aliphatic content was retrieved by mass analysis. Figure 4c-d summarizes the degree of polymerization (DP, here measured up to 14) of aromatic monomers as a function of the DP of aliphatic monomers observed in the SEC-MS experiments.

In PES2_NC sample, several congeners exist with variable DP of aliphatic acid (**5**) ranging from 0 to 4, with the aromatic DP being between 1 and 14 (**3** and **4** cannot be distinguished from each other because they are isobaric). This situation changes significantly when analyzing PES2_LCC sample. In this case, the species detected in the same molecular weight range are deprived of aliphatic acid (**5**). In particular, the assigned mono-acid terminated chains of PES2_LCC sample carry 0 to 1 aliphatic monomer and the intensities of the signals are below 10%. In contrast, the di-acid terminated chains were detected with a maximum of two aliphatic units and an intensity of 2% maximum.

Based on these observations, we conclude that the reduction in molecular weight observed by enzymatic hydrolysis is likely to occur via in-chain hydrolysis and at the sites of the aliphatic monomers rather than at the polymer end group. These results agree with the different hydrolysis rates that the enzymes exhibited toward aliphatic or aromatic homopolymers. It should be noted that the list of assignments is representative of the lower mass portion of the sample; however, we expect the same trend to apply to higher molecular weight species.

Conclusions

In this study, we described an in-depth analytical characterization of the process of hydrolysis of polyesters catalyzed by a recently described cutinase (LCC^{WCCG}) and a homologue cutinase variant that was created and reported for the first time in this work (Tc_Cut2NV^{WCCG}). Assay small molecules, aliphatic and aromatic polyesters as well as an aromatic-aliphatic co-polyester were investigated for their depolymerization with the chosen cutinases. RPLC-UV-MS analyses allowed us to monitor the water-soluble products released by hydrolysis. SEC-MS analysis allowed us to gain insight into the monomer composition of the species resulting from the enzymatic hydrolysis.

We conclude that LCC^{WCCG} and Tc_Cut2NV^{WCCG} depolymerize the constituting monomers depending on their chemicophysical characteristics such as in the case illustrated here of aliphatic and aromatic monomers. The results and method proposed herein give insights into the mode of hydrolysis of these cutinases in co-polyester systems, thereby providing information for the rational engineering of more selective and catalytically active enzymes. These results could be exploited as a starting point for developing analytical workflows in which the selectivity of enzymes is harnessed to characterize the co-polymer distribution in a polymer sequence. Additionally, the engineering of highly active enzymes for the hydrolysis of diverse synthetic polyesters holds transformative potential for many other domains. For instance, the application of these hydrolases in polymer recycling can create tangible benefits for society, ecosystems, and the economy by addressing environmental concerns, enhancing resource efficiency, and promoting sustainability and circularity. This work also demonstrates that an integrated approach involving several disciplines, such as biocatalysis, analytical chemistry, and polymer science, is crucial for fostering a more sustainable future in which better degradable polymers can be designed and synthesized, and effectively degraded by engineered enzymes at the end of their lifecycle.

Supporting Information Summary

Additional references are cited in the supporting information.[20] The online version contains supplementary material available at https://doi.org/10.1002/chem.202403879.

Credit Author Statement

E.A., V.T., J.D., A.F.G.G. and F.G.M. wrote the manuscript. E.A., V.T. and J.D. created the figures and schemes. E.A. performed depolymerization reactions; characterization analysis; data interpretation; and contributed to enzymes purification and thermostability and activity assays. V.T. performed bioinformatic analysis; enzyme mutagenesis, expression and purification; thermostability and activity assays; and all the tasks related to computational studies (homology models, dockings). A.F.G.G designed the separation and mass spectrometry method; and performed and supported data visualization and interpretation. A.F.G.G. and J.D. performed the SEC-MS measurements. J.D. performed the SEC-MS data interpretation and visualization. F.G.M. reviewed the computational structural models of the enzymes. P.B. performed the synthesis of the polymer models and the small model substrates. Masa S. performed the additional experiments with polymer PES4. Martin. S. and R.P. provided intellectual input, support to supervision, and material and resources during the implementation of the project.

A.F.G.G. and F.G.M acquired the funding, and designed and directed the research.

Acknowledgements

This research was funded by Topconsortium voor Kennis en Innovatie (TKI) Chemie, deployment project PPS-programmatoeslag 2019 (CHEMIE.PGT.2020.020). Contribution from Covestro Resins & Functional Materials, and InnoSyn B.V. are acknowledged. We thank Harry Philipsen (DSM Geleen) for the insightful discussions.

Conflict of Interests

The authors declare no conflict of interest.

Data Availability Statement

The data that support the findings of this study are available in the supplementary material of this article.

Keywords: Co-polyesters · Selective enzymatic hydrolysis · SEC-MS · Hydrolases · Biocatalysis

[1] a) E. F. Izard, *J. Polym. Sci.* **1952**, *8*, 503–518; b) M. Gilbert, F. J. Hybart, *Polymer* **1972**, *13*, 327–332; c) D. Feldman, *J. Polym. Sci., Polym. Lett. Ed.* **1985**, *23*, 493–494; d) B. Klumperman, R. Pfukwa, A. Lederer, *Statistical, Alternating, and Gradient Copolymers, in Macromolecular Engineering* (Eds: K. Matyjaszewski, Y. Gnanou, L. Leibler), Wiley-VCH Verlag GmbH & Co. KGaA, Weinheim, 813–838; e) E. F. Palermo, A. J. McNeil, *Macromolecules* **2012**, *45*, 5948–5955; f) A. J. Trazkovich, M. F. Wendt, L. M. Hall, *Soft Matter* **2018**, *14*, 5913–5921; g) C.-L. Lin, W.-C. Chen, C.-S. Liao, Y.-C. Su, C.-F. Huang, S.-W. Kuo, F.-C. Chang, *Macromolecules* **2005**, *38*, 6435–6444; h) A. B. Staubli, E. Mathiowitz, R. S. Langer, *Macromolecules* **1991**, *24*, 2291–2298; i) Y. Kametani, F. Tournilhac, M. Sawamoto, M. Ouchi, *Angew. Chem. Int. Ed.* **2020**, *59*, 5193–5201; j) D. M. Bigg, *Adv. Polym. Tech.* **2005**, *24*, 69–82.

[2] T. N. J. Fouquet, H. Pizzala, M. Rollet, D. Crozet, P. Giusti, L. Charles, *J. Am. Soc. Mass. Spectrom.* **2020**, *31*, 1554–1562.

[3] a) Q. Y. Lee, H. Li, *Micromachines* **2021**, *12*, 907; b) Y. Lin, T. B. Kouznetsova, C.-C. Chang, S. L. Craig, *Nat. Commun.* **2020**, *11*, 4987; c) R. K. Singh, B. Ruj, A. K. Sadhukhan, P. Gupta, *J. Environ. Manage.* **2019**, *239*, 395–406.

[4] a) Å. M. Ronkvist, W. Xie, W. Lu, R. A. Gross, *Macromolecules* **2009**, *42*, 5128–5138; b) K. Shi, J. Jing, L. Song, T. Su, Z. Wang, *Int. J. Biol. Macromol.* **2020**, *144*, 183–189; c) H. N. Cheng, R. A. Gross, P. B. Smith, *ACS Symposium Series*, American Chemical Society, Washington, DC **2013**; d) C. M. Carr, D. J. Clarke, A. D. Dobson, *Front. Microbiol.* **2020**, *11*, 571265; e) E. L. Bell, R. Smithson, S. Kilbride, J. Foster, F. J. Hardy, S. Ramachandran, A. A. Tedstone, S. J. Haigh, A. A. Garforth, P. J. R. Day, C. Levy, M. P. Shaver, A. P. Green, *Nat. Catal.* **2022**, *5*, 673–681; f) A. Su, T. Tyrikos-Ergas, A. N. Shirke, Y. Zou, A. L. Dooley, I. V. Pavlidis, R. A. Gross, *ACS Catal.* **2018**, *8*, 7944–7951.

[5] a) A. Mrigwani, M. Pitaliya, H. Kaur, B. Kasilingam, B. Thakur, P. Guptasarma, *Biotechnol. Bioeng.* **2023**, *120*, 674–686; b) I. Kleeberg, K. Welzel, J. VandenHeuvel, R. J. Müller, W. D. Deckwer, *Biomacromolecules* **2005**, *6*, 262–270.

[6] Z. Zhang, S. Huang, D. Cai, C. Shao, C. Zhang, J. Zhou, Z. Cui, T. He, C. Chen, B. Chen, T. Tan, *Green Chem.* **2022**, *24*, 5998–6007.

[7] V. Tournier, C. M. Topham, A. Gilles, B. David, C. Folgoas, E. Moya-Leclair, E. Kamionka, M. L. Desrousseaux, H. Texier, S. Gavalda, M. Cot, E. Guémard, M. Dalibey, J. Nomme, G. Cioci, S. Barbe, M. Chateau, I. André, S. Duquesne, A. Marty, *Nature* **2020**, *580*, 216–219.

[8] a) I. Taniguchi, S. Yoshida, K. Hiraga, K. Miyamoto, Y. Kimura, K. Oda, *ACS Catal.* **2019**, *9*, 4089–4105; b) A. Berselli, M. J. Ramos, M. C. Menziani, *ChemBioChem* **2021**, *22*, 2032–2050; c) R. Wei, G. von Haugwitz, L. Pfaff, J. Mican, C. P. S. Badenhorst, W. Liu, G. Weber, H. P. Austin, D. Bednar, J. Damborsky, U. T. Bornscheuer, *ACS Catal.* **2022**, *12*, 3382–3396; d) H. Lu, D. J. Diaz, N. J. Czarnecki, C. Zhu, W. Kim, R. Shroff, D. J. Acosta, B. R. Alexander, H. O. Cole, Y. Zhang, N. A. Lynd, A. D. Ellington, H. S. Alper, *Nature* **2022**, *604*, 662–667; e) Y. Cui, Y. Chen, X. Liu, S. Dong, Y. Tian, Y. Qiao, R. Mitra, J. Han, C. Li, X. Han, W. Liu, Q. Chen, W. Wang, X. Wang, W. Du, S. Tang, H. Xiang, H. Liu, Y. Liang, K. N. Houk, B. Wu, *ACS Catal.* **2021**, *11*, 1340–1350; f) L. Pfaff, J. Gao, Z. Li, A. Jäckering, G. Weber, J. Mican, Y. Chen, W. Dong, X. Han, C. G. Feiler, Y. F. Ao, C. P. S. Badenhorst, D. Bednar, G. J. Palm, M. Lammers, J. Damborsky, B. Strodel, W. Liu, U. T. Bornscheuer, R. Wei, *ACS Catal.* **2022**, *12*, 9790–9800; g) H. F. Son, I. J. Cho, S. Joo, H. Seo, H.-Y. Sagong, S. Y. Choi, S. Y. Lee, K.-J. Kim, *ACS Catal.* **2019**, *9*, 3519–3526; h) B. Eiamthong, P. Meesawat, T. Wongsatit, J. Jitdee, R. Sangsri, M. Patchsung, K. Aphicho, S. Suraritdechachai, N. Huguenin-Dezot, S. Tang, W. Suginta, B. Paosawatyanyong, M. M. Babu, J. W. Chin, D. Pakotiprapha, W. Bhanthumnavin, C. Uttamapinant, *Angew. Chem. Int. Ed.* **2022**, *61*, e202203061; i) K. Chen, Y. Hu, X. Dong, Y. L. Sun, *ACS Catal.* **2021**, *11*, 7358–7370; j) A. Nakamura, N. Kobayashi, N. Koga, R. Iino, *ACS Catal.* **2021**, *11*, 8550–8564; k) S. Brott, L. Pfaff, J. Schuricht, J. N. Schwarz, D. Böttcher, C. P. S. Badenhorst, R. Wei, U. T. Bornscheuer, *Eng. Life Sci.* **2022**, *22*, 192–203; l) W. Zeng, X. Li, Y. Yang, J. Min, J.-W. Huang, W. Liu, D. Niu, X. Yang, X. Han, L. Zhang, L. Dai, C.-C. Chen, R.-T. Guo, *ACS Catal.* **2022**, *12*, 3033–3040; m) G. Arnal, J. Anglade, S. Gavalda, V. Tournier, N. Chabot, U. T. Bornscheuer, G. Weber, A. Marty, *ACS Catal.* **2023**, *13*, 13156–13166.

[9] a) U. Witt, R.-J. Müller, W.-D. Deckwer, *J. Environ. Polym. Degrad.* **1997**, *5*, 81–89; b) U. Witt, M. Yamamoto, U. Seeliger, R. J. Müller, V. Warzelhan, *Angew. Chem. Int. Ed.* **1999**, *38*, 1438–1442; c) E. Marten, R.-J. Müller, W.-D. Deckwer, *Polym. Degrad. Stab.* **2005**, *88*, 371–381; d) E. Marten, R.-J. Müller, W.-D. Deckwer, *Polym. Degrad. Stab.* **2003**, *80*, 485–501; e) I. Kleeberg, K. Welzel, J. Vandenheuvel, R. J. Müller, W. D. Deckwer, *Biomacromolecules* **2005**, *6*, 262–270.

[10] E. Herrero Acero, D. Ribitsch, A. Dellacher, S. Zitzenbacher, A. Marold, G. Steinkellner, K. Gruber, H. Schwab, G. M. Guebitz, *Biotechnol. Bioeng.* **2013**, *110*, 2581–2590.

[11] a) R. Wei, W. Zimmermann, *Microb. Biotechnol.* **2017**, *10*, 1302–1307; b) R. Wei, T. Oeser, J. Then, N. Kühn, M. Barth, J. Schmidt, W. Zimmermann, *AMB Express* **2014**, *4*, 44.

[12] D. Ribitsch, A. Hromic, S. Zitzenbacher, B. Zartl, C. Gamerith, A. Pellis, A. Jungbauer, A. Lyskowski, G. Steinkellner, K. Gruber, R. Tscheliessnig, E. Herrero Acero, G. M. Guebitz, *Biotechnol. Bioeng.* **2017**, *114*, 2481–2488.

[13] a) B. Liu, L. He, L. Wang, T. Li, C. Li, H. Liu, Y. Luo, R. Bao, *ChemBioChem* **2018**, *19*, 1471–1475; b) Z. Chen, Y. Wang, Y. Cheng, X. Wang, S. Tong, H. Yang, Z. Wang, *Sci. Total Environ.* **2020**, *709*, 136138; c) S. Yoshida, K. Hiraga, T. Takehana, I. Taniguchi, H. Yamaji, Y. Maeda, K. Toyohara, K. Miyamoto, Y. Kimura, K. Oda, *Science* **2016**, *351*, 1196–1199.

[14] N. Lucas, C. Bienaime, C. Belloy, M. Queneudec, F. Silvestre, J. E. Nava-Saucedo, *Chemosphere* **2008**, *73*, 429–442.

[15] I. Roszak, L. Oswald, A. Al Ouahabi, A. Bertin, E. Laurent, O. Felix, I. Carvin-Sergent, L. Charles, J. F. Lutz, *Polym. Chem.* **2021**, *12*, 5279–5282.

[16] S. R. A. Molenaar, B. van de Put, J. S. Desport, S. Samanipour, R. A. H. Peters, B. W. J. Pirok, *Anal. Chem.* **2022**, *94*, 5599–5607.

[17] a) J. Song, J. W. van Velde, L. L. T. Vertommen, D. F. Smith, R. M. A. Heeren, O. F. van den Brink, *Macromolecules* **2011**, *44*, 1319–1326; b) K. De Bruycker, A. Welle, S. Hirth, S. J. Blanksby, C. Barner-Kowollik, *Nat. Rev. Chem.* **2020**, *4*, 257–268.

[18] K. M. Saller, I. Gnatiuk, D. Holzinger, C. Schwarzinger, *Anal. Chem.* **2020**, *92*, 15221–15228.

[19] J. S. Desport, G. Frache, L. Patiny, *Rapid Commun. Mass Spectrom.* **2020**, *34*, e8652.

[20] a) E. Krieger, G. Koraimann, G. Vriend, *Proteins* **2002**, *47*, 393–402; b) C. Oostenbrink, A. Villa, A. E. Mark, W. F. van Gunsteren, *J. Comput. Chem.* **2004**, *25*, 1656–1676; c) H.-S. Yang, J.-S. Yoon, M.-N. Kim, *Polym. Degrad. Stab.* **2005**, *87*, 131–135.

Manuscript received: October 21, 2024
Accepted manuscript online: February 12, 2025